



ChemComm

**Solution-Phase Synthesis of the Chalcogenide Perovskite
Barium Zirconium Sulfide as Colloidal Nanomaterials**

Journal:	<i>ChemComm</i>
Manuscript ID	CC-COM-06-2022-003494.R1
Article Type:	Communication

SCHOLARONE™
Manuscripts

COMMUNICATION

Solution-Phase Synthesis of the Chalcogenide Perovskite Barium Zirconium Sulfide as Colloidal Nanomaterials

Daniel Zilevu, Omri O. Parks, Sidney E. Creutz*

Received 00th January 20xx,
Accepted 00th January 20xx

DOI: 10.1039/x0xx00000x

Chalcogenide perovskites such as BaZrS_3 have promising optoelectronic properties. Methods to produce these materials at low temperatures, especially in the solution phase, are currently scarce. We describe a solution-phase synthesis of colloidal nanoparticles of BaZrS_3 using reactive metal amide precursors. The nanomaterials are crystallographically and spectroscopically characterized.

The search for efficient and low-cost materials for thin-film photovoltaics has in recent years been dominated by a focus on hybrid lead halide perovskites due to their low cost, facile processing, and high efficiency—exceeding 29% when combined with silicon in a tandem device.¹ However, concerns about the stability, toxicity, and potential environmental effects of these lead-based materials have already begun to drive substantial research efforts towards the development of related materials with higher stability and lower toxicity.^{2–4} Among the many proposed materials, chalcogenide perovskites and related materials with general formula ABQ_3 (A = Ca, Ba, Sr; B = Zr, Hf, Ti; Q = S, Se) show particularly strong promise based on their optoelectronic properties and excellent stability.^{5–7} Of these materials, BaZrS_3 has drawn the most attention because of its distorted perovskite structure and useful optical properties (Figure 1A). In particular, at ~ 1.8 eV its bandgap is higher than the ideal for a single-junction solar cell but competitive to replace perovskites in tandem applications; moreover, the bandgap could be lowered closer to the ideal by alloying or the use of related Ruddlesden-Popper phases.^{6,8–11}

Despite the theorized potential of BaZrS_3 , development and testing of it in thin-film devices has been largely hindered by the lack of low-temperature methods to deposit it as a thin film.⁶ The first bulk syntheses of BaZrS_3 required temperatures near or above 1000 °C.^{12,13} Further tuning of the chemistry and

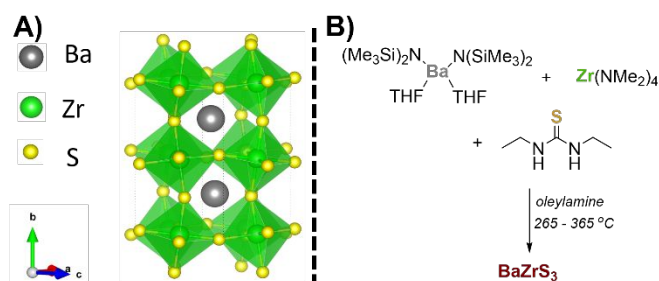


Figure 1. (A) Depiction of the crystal structure of the orthorhombic perovskite BaZrS_3 . (B) Synthetic scheme for the synthesis of BaZrS_3 nanoparticles.

stoichiometry eventually lowered this to 450 °C.^{14,15} Initial efforts to generate BaZrS_3 thin films have relied on sulfurization of oxide films or co-sputtering approaches, but high temperatures (>900 °C) were usually needed to complete the reaction and achieve crystalline materials.^{16–18} Recently, epitaxial film growth has been achieved at lower temperatures (>700 °C) using pulsed laser deposition.¹⁹ Most promisingly, film growth and crystallization at 600 °C has been achieved using a sputtering/sulfurization approach.²⁰ Many of these techniques also require more complex and expensive equipment compared to the *solution-phase* growth and processing that is possible with the hybrid lead halide perovskites.

The solution-phase synthesis of chalcogenide perovskites as nanomaterials represents a potential alternative route to their preparation that might be amenable to lower synthesis temperatures. There has been one report of the successful preparation of colloidal BaZrS_3 nanoparticles by grinding bulk BaZrS_3 to a fine powder and treating it with appropriate solvents/ligands to extract a population of small (40–60 nm) colloidal particles, which were successfully processed into thin-film devices.²¹ However, methods for the *direct* solution-phase synthesis of BaZrS_3 nanomaterials are still lacking.

In this communication, we report the synthesis of BaZrS_3 as colloidal nanoparticles using reactive metal amide precursors in oleylamine solution, with N,N'-diethylthiourea as the sulfur source, using a procedure adapted from that we previously

Department of Chemistry, Mississippi State University, Mississippi State, MS 39762, United States

Email: screutz@chemistry.msstate.edu

Electronic Supplementary Information (ESI) available: Detailed experimental procedures and additional characterization data. See DOI: 10.1039/x0xx00000x

reported for the synthesis of BaTiS₃ nanomaterials.²² The reaction was successful at temperatures ranging from 365 °C to as low as 275 °C. However, nanomaterials synthesized at the lower temperatures showed structural distortions and a more pronounced platelet-like morphology as compared to those synthesized at the upper end of the temperature range.

Briefly, in a typical synthesis, Ba[N(TMS)₂]₂(THF)₂,²³ Zr[N(CH₃)₂]₄, and N,N'-diethylthiourea are combined in a 1:2:60 mole ratio in rigorously dried oleylamine, at a concentration of 0.08 M in Ba²⁺ (Figure 1B). The reaction is carried out in a Schlenk reaction tube under inert gas using a set-up similar to that we previously reported for the heat-up synthesis of BaTiS₃.²⁴ The reaction mixture is heated to the desired reaction temperature (e.g., 365 °C) and maintained at this temperature for 30 minutes before being allowed to cool to room temperature. During heating, the reaction mixture takes on a deep red-brown color and remains homogeneous in appearance. Following precipitation and washing of the nanomaterials from the reaction solution using anhydrous chloroform and ethanol, BaZrS₃ nanoparticles are isolated as an orange-red powder.

We found that a large excess of the sulfur precursor and a high concentration in solution were both important for the success of the reaction; otherwise, impurity phases were commonly observed. Additionally, the use of the readily soluble and reactive metal amide precursors greatly facilitated the successful production of crystalline BaZrS₃. Attempts to synthesize this material using simple chloride and acetate salts of Ba²⁺ and Zr⁴⁺ have thus far been unsuccessful in our hands, as have attempts to use alternative sulfur precursors including CS₂ and (Me₃Si)₂S; in these cases, binary phases such as BaS and ZrS₂ are frequently observed, or no detectable crystalline phase is observed at all. Although the synthesis itself must be carried out under rigorously anhydrous conditions due to the reactive nature of the precursors, the resulting nanomaterials are quite stable to air and moisture (*vide infra*). However, the initial nanoparticle purification must also be carried out under air- and water-free conditions in order to avoid contamination of the sample with amorphous oxide byproducts (e.g. ZrO₂).

Figure 2 shows characterization data for a sample of nanoparticles obtained at the highest readily accessible temperature—approximately 365 °C, corresponding to vigorously refluxing oleylamine. Figure 2A compares the powder diffraction pattern of the nanoparticles to the predicted pattern based on the reported orthorhombic distorted perovskite structure of bulk BaZrS₃; the diffraction peak positions are reasonably well-matched, with the expected size-related broadening.²⁵ TEM imaging (Figure 2B-C) shows nano-sized particles which appear to have a plate-like morphology and tend to be highly aggregated, making precise size distribution measurements challenging. Typically, the particles are non-uniform and polydisperse with the majority of particles falling within a lateral size range from approximately 10 to 40 nm; this is corroborated by fitting of the PXRD data to a model incorporating uniaxial size broadening (Figures S10-S11 in the Supplementary Information). Lattice fringes observed in TEM images of the material (Figure S14) suggest that the observed

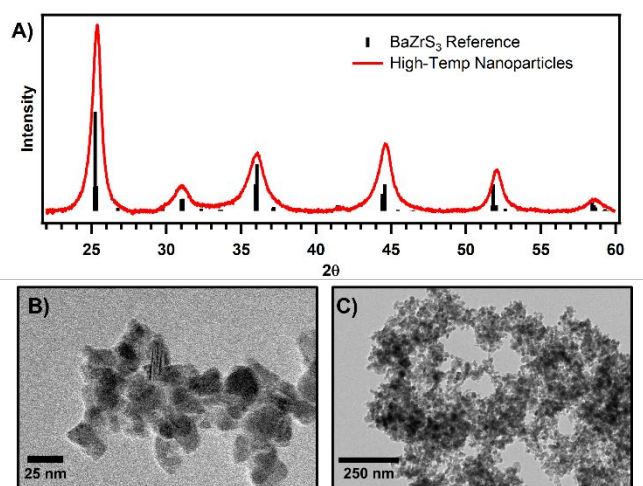


Figure 2. Structural characterization and imaging of HT-BaZrS₃ nanomaterials. (A) PXRD pattern of synthesized orthorhombic BaZrS₃ nanoparticles (red), compared to calculate reference pattern (black). (B, C) TEM images of the same nanoparticles, at two different magnification levels.

particles are crystalline, and polycrystalline electron diffraction measurements (see Figures S12-S13) are consistent with the structure of BaZrS₃ as observed by PXRD.

EDX measurements carried out on a sample of BaZrS₃ nanomaterials gave a percent atomic composition in reasonable agreement with the expected values for BaZrS₃ (Figure 3); elemental mapping shows that these elements are uniformly distributed across the sample, suggesting a homogeneous ternary phase. The sample shown is slightly enriched in barium relative to zirconium, which is typical in most of our samples measured by EDX. Elemental analysis by ICP-MS of a similarly prepared nanocrystal sample after acid digestion also gave close to the stoichiometric ratio of Ba:Zr, but slightly enriched in Zr (1:1.2 Ba:Zr); the reason for this discrepancy is not clear but could be related to different sample preparation methods for the two elemental analysis techniques (EDX vs. ICP).

These nanomaterials, synthesized at the high-temperature limit, are referred to as HT-BaZrS₃ in the following discussion. Characterization data for additional nanocrystal samples synthesized under these conditions are provided in the Supplementary Information (Table S2, Figures S3-S5).

The temperature dependence of the reaction was canvassed by carrying out the reaction at temperatures from 250 °C to 365 °C (Figure S8). At temperatures of 275 °C and above, a red-brown nanocrystalline powder was obtained following work-up; no crystalline material was produced from a reaction at 250 °C. While the HT-BaZrS₃ nanomaterials

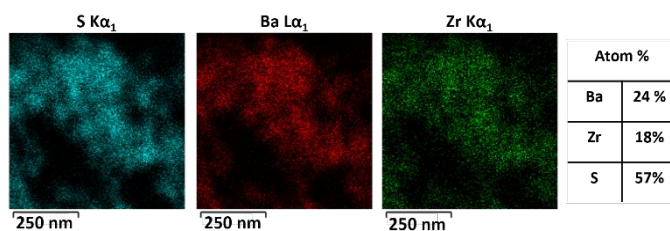


Figure 3. Elemental mapping of S, Ba, and Zr on a cluster of nanoparticles in a HT-BaZrS₃ TEM sample, using energy-dispersive X-ray spectroscopy (EDX). Atomic percentages determined from this data (averaged over the area shown) are given on the left.

discussed above (Figure 2) showed a good structural match to bulk orthorhombic BaZrS_3 , syntheses carried out at lower temperatures showed some apparent structural changes (Figure 4); we refer to these material as LT- BaZrS_3 . We note that this result was also sometimes observed in nanoparticle samples synthesized at 365 °C for reasons that are not currently clear. Powder X-ray diffraction analysis of these nanomaterials showed evidence of deviations from the reported bulk structure, as illustrated in Figure 4A. Key differences include the presence of additional diffracted intensity around $2\theta = 34^\circ$ and 22.5° , along with small shifts of the other major diffraction peaks towards higher angles and the appearance of a broad shoulder on the low-angle side of the peak near 44.5° . The Ruddlesden-Popper $\text{Ba}_3\text{Zr}_2\text{S}_7$ and Ba_2ZrS_4 phases do not appear to be a better match to the experimental data (Figure 4A).^{26,27} It is difficult to completely rule out that the samples could actually be a mixture of related phases, although they do appear uniform by TEM (Figure 4B-C).

TEM imaging (Figure 4B-C) of LT- BaZrS_3 shows nanoplatelet-like particles. Elemental analysis (EDX) data is similar to that measured for HT- BaZrS_3 , although the samples tend to have a higher barium/zirconium ratio. Given the platelet-like morphology of the particles, this discrepancy could be partly accounted for if the lateral surface planes are Ba/S-rich. However, we cannot conclusively determine if this is the case.

To better understand the origin of the apparent structural distortions, and to further confirm the identity of the material as a distorted perovskite BaZrS_3 , preliminary structural refinement was carried out using atomic pair distribution function (PDF) analysis of synchrotron-based X-ray scattering data (see Supplementary Information, Figure S15 and Table S5, for details and fit parameters). The resulting data and fits are shown in Figure 5. Data from the high-temperature particles (HT- BaZrS_3) are shown in Figure 5a, overlaid with a fit to the bulk BaZrS_3 structure. During the fitting, refinement of the lattice parameters and isotropic atomic displacement parameters was allowed while other structural parameters were fixed to those

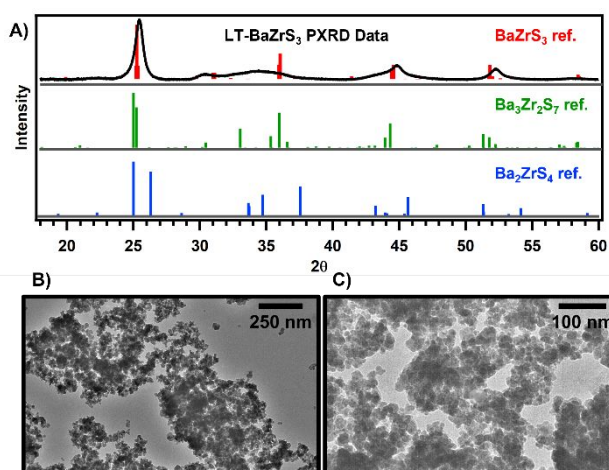


Figure 4. Structural characterization and imaging data for LT- BaZrS_3 nanomaterials (see text for discussion). (A) Measured PXRD pattern (black) compared to calculated reference patterns for orthorhombic BaZrS_3 and two related Ruddlesden-Popper phases. (B, C) TEM images of the nanomaterial sample at two different magnification levels.

of the reported bulk structure. Overall the PDF data appears consistent with a $Pnma$ distorted perovskite BaZrS_3 structure.

Figure 5B shows PDF data for a representative sample of LT- BaZrS_3 , with corresponding fits to the perovskite BaZrS_3 structure; while the peak positions generally match at low r values, there are more discrepancies in the intensities, and the fit at higher r values becomes poor, suggesting changes to the overall structure relative to the HT- BaZrS_3 sample. For further comparison, attempted fits of this PDF data to the reported structures of $\text{Ba}_3\text{Zr}_2\text{S}_7$ and Ba_2ZrS_4 are shown in Figure 5C and by visual inspection are less successful than the fit to BaZrS_3 ; these fits also have higher R_w values (Table S5). Therefore, the PDF data suggests that these nanoparticles may still possess the perovskite-like structure of bulk BaZrS_3 at least on the local level. The exact nature of the structural distortions suggested by PXRD and PDF analysis, and their relationship to the particle morphology and synthesis temperature, is not yet known; investigations into this question are ongoing and will be elaborated in future reports.

Figure 6A shows an absorbance spectrum for a colloidal solution of the HT- BaZrS_3 nanoparticles. The spectrum shows a shallow sloping onset around 750 nm and a steeper slope commencing around 600 nm. A broad shoulder is detectable at 460 nm, and an additional peak at 300 nm. The absorption onset is in line with those reported in the literature for bulk BaZrS_3 , and is also reflected by the reddish-orange color of the materials (Figure 6B-C).⁶ The exact value of the intrinsic band gap for BaZrS_3 is not well-established, with reports ranging at

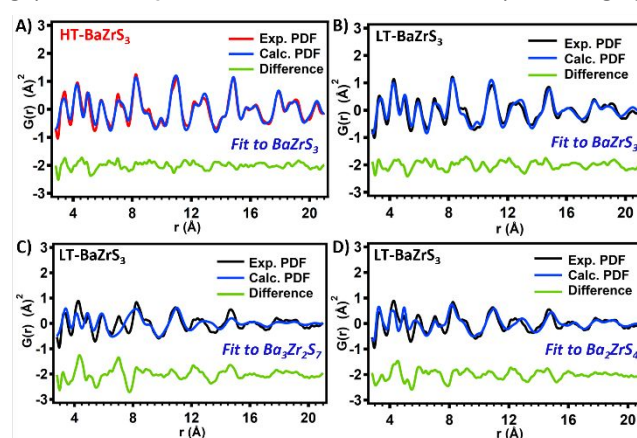


Figure 5. Pair distribution function data for HT- BaZrS_3 (A) and LT- BaZrS_3 (B-D). Data is shown in black, fits to the indicated phases are shown in blue, and the difference curves are shown in green.

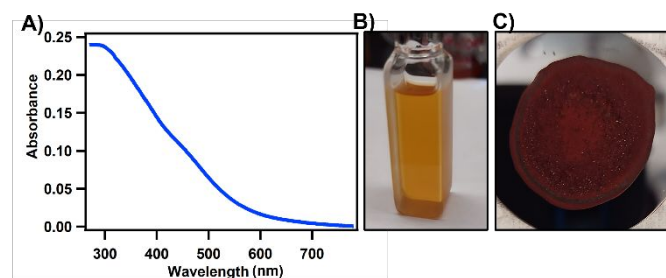


Figure 6. Optical properties of the BaZrS_3 nanomaterials. (A) UV-visible absorbance spectrum of a colloidal solution of nanoparticles in chloroform. (B) Photograph of a dilute dispersion of the nanoparticles in chloroform. (C) Photograph of a drop-cast nanoparticle powder on a silicon substrate.

least from 1.75 eV to 1.94 eV.^{18,28} Unfortunately, we were unable to detect significant luminescence from our materials; it has been noted that the luminescence of BaZrS₃ nanomaterials can be highly dependent on surface treatment, so further optimization of the surface termination could elicit emission in the future.²¹

Finally, we tested the stability of the nanoparticles to exposure to ambient atmosphere and to direct immersion in water, to determine if the excellent stability observed for bulk BaZrS₃ might hold true on the nanoscale (Figure 7). For a sample of HT-BaZrS₃, the PXRD pattern did not change significantly over the course of 9 weeks of exposure to ambient atmosphere. Upon immersion in water, a small unidentified impurity peak was observed in the sample after 30 minutes. Therefore, although the stability of these nanomaterials against water is higher than that of lead halide perovskite nanocrystals or BaTiS₃ nanocrystals,²⁴ they may be less resilient than bulk BaZrS₃.

In conclusion, we have demonstrated that colloidal suspensions of BaZrS₃ nanomaterials can be obtained using a low-temperature, solution-phase process. The approaches reported here may be generalizable to other related materials.

This work was supported by the National Science Foundation of the United States (Grant #2004421). Bruno Donnadiu is thanked for assistance with PXRD measurements and Dr. Roobanvenkatesh Thirulamai for assistance with TEM, EDX, and electron diffraction measurements. This research used the mail-in program at Beamline 11-ID-B of the Advanced Photon Source, a U.S. Department of Energy (DOE) Office of Science User Facility, operated for the DOE Office of Science by Argonne National Laboratory under Contract No. DE-AC02-06CH11357. Dr. Leighanne Gallington is thanked for assistance with collecting synchrotron X-ray total scattering data.

There are no conflicts of interest to declare.

Notes and references

- 1 A. Al-Ashouri, E. Köhnen, B. Li, A. Magomedov, H. Hempel, P. Caprioglio, J. A. Márquez, A. B. Morales Vilches, E. Kasparavicius, J. A. Smith, N. Phung, D. Menzel, M. Grischek, L. Kegelman, D. Skroblin, C. Gollwitzer, T. Malinauskas, M. Jošt, G. Matič, B. Rech, R. Schlatmann, M. Topič, L. Korte, A. Abate, B. Stannowski, D. Neher, M. Stolterfoht, T. Unold, V. Getautis and S. Albrecht, *Science*, 2020, **370**, 1300–1309.
- 2 A. M. Ganose, C. N. Savory and D. O. Scanlon, *Chem. Commun.*, 2016, **53**, 20–44.
- 3 A. H. Slavney, R. W. Smaha, I. C. Smith, A. Jaffe, D. Umeyama and H. I. Karunadasa, *Inorg. Chem.*, 2017, **56**, 46–55.
- 4 R. E. Brandt, V. Stevanović, D. S. Ginley and T. Buonassisi, *MRS Commun.*, 2015, **5**, 265–275.
- 5 A. Swarnkar, W. J. Mir, R. Chakraborty, M. Jagadeeswararao, T. Sheikh and A. Nag, *Chem. Mater.*, 2019, **31**, 565–575.
- 6 K. V. Sopiha, C. Comparotto, J. A. Márquez and J. J. S. Scragg, *Adv. Opt. Mater.*, 2022, **10**, 2101704.
- 7 S. Niu, J. Milam-Guerrero, Y. Zhou, K. Ye, B. Zhao, B. C. Melot and J. Ravichandran, *J. Mater. Res.*, 2018, **33**, 4135–4143.
- 8 W. Meng, B. Saparov, F. Hong, J. Wang, D. B. Mitzi and Y. Yan, *Chem. Mater.*, 2016, **28**, 821–829.
- 9 S. Niu, D. Sarkar, K. Williams, Y. Zhou, Y. Li, E. Bianco, H. Huyan, S. B. Cronin, M. E. McConney, R. Haiges, R. Jaramillo, D. J. Singh, W. A. Tisdale, R. Kapadia and J. Ravichandran, *Chem. Mater.*, 2018, **30**, 4882–4886.
- 10 S. Niu, H. Huyan, Y. Liu, M. Yeung, K. Ye, L. Blankemeier, T. Orvis, D. Sarkar, D. J. Singh, R. Kapadia and J. Ravichandran, *Adv. Mater.*, 2017, **29**, 1604733.
- 11 W. Li, S. Niu, B. Zhao, R. Haiges, Z. Zhang, J. Ravichandran and A. Janotti, *Phys. Rev. Materials*, 2019, **3**, 101601.
- 12 A. Clearfield, *Acta Cryst.*, 1963, **16**, 135–142.
- 13 H. Hahn and U. Mutschke, *Z. Anorg. Allg. Chem.*, 1957, **288**, 269–278.
- 14 Y. Wang, N. Sato and T. Fujino, *J. Alloys Compd.*, 2001, **327**, 104–112.
- 15 Y. Wang, N. Sato, K. Yamada and T. Fujino, *J. Alloys Compd.*, 2000, **311**, 214–223.
- 16 C. Comparotto, A. Davydova, T. Ericson, L. Riekehr, M. V. Moro, T. Kubart and J. Scragg, *ACS Appl. Energy Mater.*, 2020, **3**, 2762–2770.
- 17 X. Wei, H. Hui, C. Zhao, C. Deng, M. Han, Z. Yu, A. Sheng, P. Roy, A. Chen, J. Lin, D. F. Watson, Y.-Y. Sun, T. Thomay, S. Yang, Q. Jia, S. Zhang and H. Zeng, *Nano Energy*, 2020, **68**, 104317.
- 18 T. Gupta, D. Ghoshal, A. Yoshimura, S. Basu, P. K. Chow, A. S. Lakhnot, J. Pandey, J. M. Warrender, H. Efstathiadis, A. Soni, E. Osei-Agyemang, G. Balasubramanian, S. Zhang, S.-F. Shi, T.-M. Lu, V. Meunier and N. Koratkar, *Adv. Funct. Mater.*, 2020, **30**, 2001387.
- 19 M. Surendran, H. Chen, B. Zhao, A. S. Thind, S. Singh, T. Orvis, H. Zhao, J.-K. Han, H. Htoon, M. Kawasaki, R. Mishra and J. Ravichandran, *Chem. Mater.*, 2021, **33**, 7457–7464.
- 20 C. Comparotto, P. Ström, O. Donzel-Gargand, T. Kubart and J. J. S. Scragg, *ACS Appl. Energy Mater.*, 2022, **5**, 6335–6343.
- 21 V. K. Ravi, S. H. Yu, P. K. Rajput, C. Nayak, D. Bhattacharyya, D. S. Chung and A. Nag, *Nanoscale*, 2021, **13**, 1616–1623.
- 22 D. Zilevu and S. E. Creutz, *Chem. Mater.*, 2021, **33**, 5137–5146.
- 23 B. A. Vaartstra, J. C. Huffman, W. E. Streib and K. G. Caulton, *Inorg. Chem.*, 1991, **30**, 121–125.
- 24 N. E. Ingram, B. J. Jordan, B. Donnadiu and S. E. Creutz, *Dalton Trans.*, 2021, **50**, 15978–15982.
- 25 R. Lelieveld and D. J. W. IJdo, *Acta Cryst B*, 1980, **36**, 2223–2226.
- 26 Y.-C. Hung, J. C. Fetters and B. W. Eichhorn, *Acta Cryst. C*, 1997, **53**, 827–829.
- 27 M. Saeki, Y. Yajima and M. Onoda, *J. Solid State Chem.*, 1991, **92**, 286–294.
- 28 Y. Nishigaki, T. Nagai, M. Nishiwaki, T. Aizawa, M. Kozawa, K. Hanzawa, Y. Kato, H. Sai, H. Hiramatsu, H. Hosono and H. Fujiwara, *Solar RRL*, 2020, **4**, 1900555.

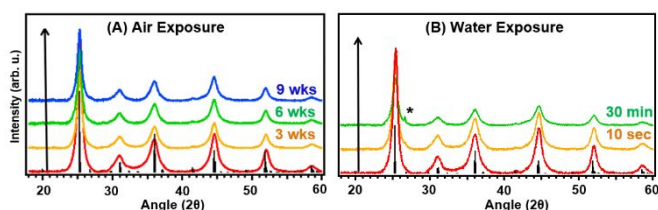


Figure 7. Stability tests on powders of BaZrS₃ nanomaterials. Black sticks represent the calculated reference pattern for BaZrS₃. (A) Exposed to ambient air over the course of 9 weeks. (B) Immersed in water for up to 30 minutes.